

in conjunction with a northwestward tilting band of off-equatorial convection that extends to near 20°N. As the entire system of convection moves to the east, the tilted structure of the off-equatorial convection band generates an apparent northward movement along individual meridians.

Section 1.2.3 provided a brief summary of the potential causes of the strong interannual variability of the South Asian monsoon. The interannual fluctuations are variously attributed to a wide variety of relationships, from ENSO to Eurasian snow cover.

Another potential source of interannual fluctuations in South Asian monsoon strength is interannual variations of intraseasonal oscillation activity. Such is the case for the Australian monsoon for which Hendon (1999) found that global ISO activity during boreal winter is inversely related to Australian monsoon strength. In other words, winter seasons that are characterized by strong and numerous intraseasonal oscillations tend to correspond to seasons of reduced north Australian monsoon rainfall. However, the ISO is considerably stronger and more regular during northern winter (e.g., Madden 1986; Hendon and Salby 1994) and the Australian monsoon is located closer to the equator, where the ISO is most influential, than the South Asian monsoon.

Nevertheless, a number of authors have observed year-to-year variability in the strength and character of the summertime ISO. Yasunari (1980) observed that the characteristic period of oscillation dropped significantly to near 60 days during the summer of 1972, a severe drought year in India, compared to the typical 40 day period. Mehta and Krishnamurti (1988) found that certain summers exhibit regular northward propagation of convection whereas during other summers the northward propagation is irregular or absent entirely. Singh *et al.* (1992) found that the

seasonal ISO intensity varies by half to double its average intensity. Chowdhury *et al.* (1988) showed, from limited data, that the interannual variability of the ISO activity is related to the overall performance of the monsoon. Ferranti *et al.* (1997), using data from five 10-year European Center for Medium-Range Weather Forecasts (ECMWF), found that intraseasonal and interannual fluctuations have a common dominant mode of variability in the Asian monsoon region.

An example of year-to-year changes in summertime ISO behavior is demonstrated in Fig. 4.1, which displays daily timeseries of precipitation over central India for the 1987 and 1988 summers, and in Fig. 4.2, which shows time-latitude sections of precipitation along 75° – 80° E for the same two seasons. The 1987 summer season is marked by three distinct active periods each separated by about 40 days. Comparison to the time-latitude section in Fig. 4.2 reveals that all three active periods over central India are associated with northward propagating systems of precipitation. Conversely, during the 1988 summer season, no well-defined active or break periods are discernible. Instead, the precipitation timeseries is marked by relatively steady rainfall from one day to the next throughout the season. In particular, the 1988 summer is largely devoid of low rainfall days. Moreover, evidence of coherent northward propagation is absent. Vernekar *et al.* (1993) found a marked difference in ISO intensity between the 1987, when ISO activity was high, and 1988, when ISO activity was virtually absent.

Previous studies of interannual variations of ISO activity have searched for a relationship with ENSO. Hendon *et al.* (1999) and Slingo *et al.* (1999) found that the amplitude of wintertime ISO activity is essentially uncorrelated with tropical eastern Pacific SST anomalies or any other SST anomalies for that matter. However, there does appear to be a detectable eastward displacement of wintertime

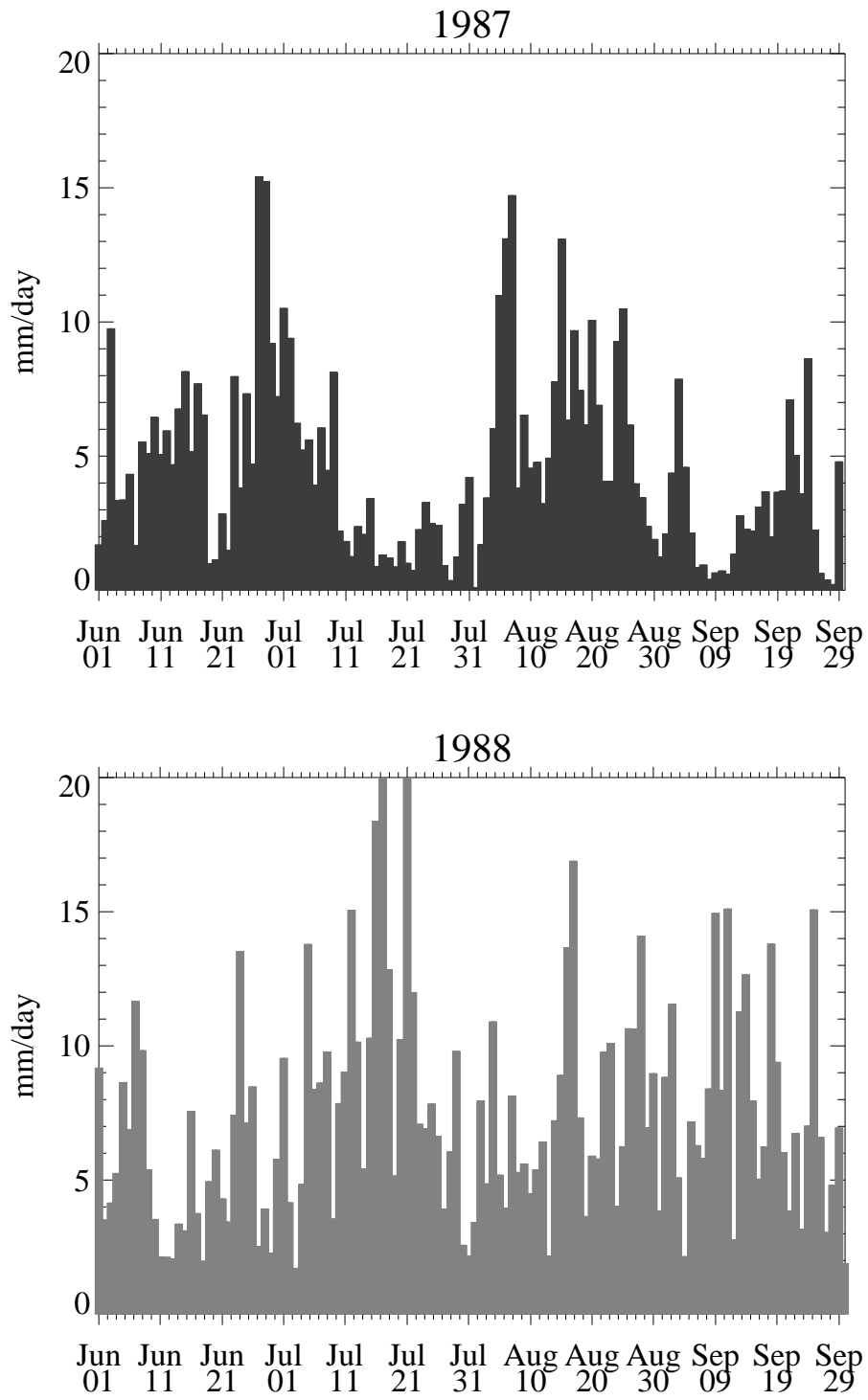


Figure 4.1. Timeseries of daily precipitation rate estimates averaged over 75° – 80° E, 10° – 15° N for June through September, 1987 and 1988.

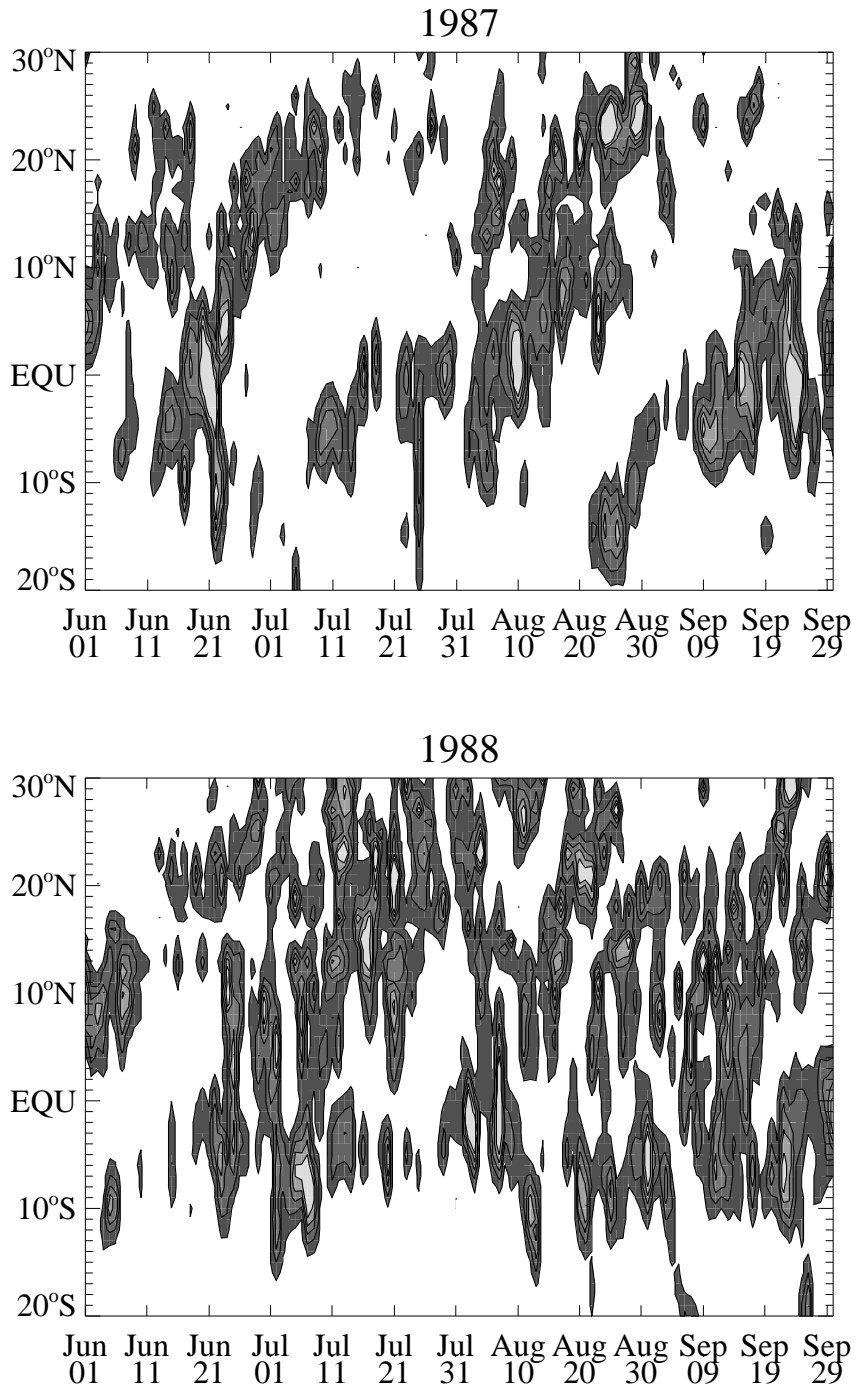


Figure 4.2. Time-latitude section of daily precipitation rate estimates along 75°–80°E for June through September, 1987 and 1988. Contour interval is 5 mm day⁻¹ with the first contour at 5 mm day⁻¹.

ISO activity during a warm ENSO event (Gutzler 1991; Fink and Speth 1997; Hendon *et al.* 1999). The relationship between ENSO and summertime ISO activity is not as well understood; but through experiments with a 5-level global spectral model, Krishnan and Kasture (1996) found that the northward propagation of convection is more regular and of slower period for warm ENSO experiments.

This chapter begins, in Section 4.2, with a description of two objective measures of summertime ISO activity. Section 4.3 introduces the various monsoon strength indices that are used and briefly examines the monsoon-ENSO relationship according to these indices. The ISO activity indices are subsequently used in Section 4.4 to explore the intricate relationships between summertime ISO activity, ENSO, and the Indian monsoon. Section 4.5 is devoted to a summary and discussion of the results of this chapter.

4.2 Measures of Boreal Summer ISO Activity

In this section, two objective indices representing the seasonal mean ISO convective activity are developed using daily-averaged OLR data. A primary limitation on studies of interannual variability of ISO activity in the past has been the lack of availability of a long term global data record that is suitable to resolve the ISO. The OLR data record is currently long enough that interannual variability studies can be conducted with a reasonable degree of confidence in the results.

Simple correlations are used to diagnose the relationships between interannual ISO variability, ENSO, and South Asian monsoon strength. Making use of the two-tailed Student's *t* test, the minimum significant correlation coefficient, r_p , can be defined as

$$r_p = \frac{t_p}{\sqrt{N - 2 + t_p^2}} \quad (4.1)$$

where p is the desired probability value, N is the degrees of freedom (d.o.f.) of the interannual timeseries, and t is the cutoff value in a Student's t distribution for the specified probability and d.o.f.. Assuming 22 d.o.f. (one for each year), the r_p correlation coefficients are 0.28, 0.36, and 0.49 for the 90%, 95%, and 99% probability levels, respectively. These values say that the absolute value of the correlation coefficient between two interannual indices must be greater than 0.36 to be considered, at a probability of 95%, to be distinct from a zero correlation.

Two methods of filtering are used to isolate the OLR signal associated with the northern summer ISO. The first method is based on the results of Section 3.2.2 which showed that at both equatorial and Indian subcontinent latitudes, low-frequency intraseasonal OLR variance is concentrated in the 25–80-day period band at eastward wavenumbers 1 through 3. Therefore, a wavenumber-frequency filter is applied to the global OLR dataset, retaining periods of 25–80 days and eastward wavenumbers 1 through 6. The range of zonal wavenumbers is broader than that of Section 3.2.2 so that interannual displacements of variance can be better captured. Hereafter in this chapter, the wavenumber-frequency filtered OLR will be referred to as OLR_{25-80e} , where the "25-80" denotes the retained period range and the "e" reflects the retained zonal wavenumbers, 1 through 6.

The second filtering method employs an empirical orthogonal function (EOF) analysis of intraseasonally filtered (25–80 days) OLR (OLR_{25-80}). The EOFs are calculated using extended summer, May to October, intraseasonally filtered data (bandpass filtered retaining periods 25–80 days, OLR_{25-80}) from a limited domain that encompasses the South Asian monsoon region and includes the area of maximum tropical eastern hemisphere OLR_{25–80} variance (40° – 180° E, 20° S– 30° N, see Fig. 4.7a). The leading two EOFs, shown in Fig. 4.3a, are not separable according

to the criteria suggested by North *et al.* (1982). Two eigenmodes can be considered inseparable if the corresponding eigenvalue λ_n is not well separated from the neighboring ones; that is,

$$\delta\lambda_{n-1} < \Delta\lambda_{n-1} \quad \text{and} \quad \delta\lambda_n < \Delta\lambda_n, \quad (4.2)$$

where

$$\delta\lambda_{n-1} = \lambda_n(2/L)^{1/2} \quad (4.3)$$

is the sampling error of λ_n , $\Delta\lambda_n = \lambda_n - \lambda_{n+1}$ is the eigenvalue increment, and L is the estimated effective d.o.f.. If $\delta\lambda_n \geq \Delta\lambda_n$, but $\delta\lambda_{n-1} > \Delta\lambda_{n-1}$ and $\delta\lambda_{n+1} > \Delta\lambda_{n+1}$, then the two eigenmodes n and $n + 1$ are a pair that likely represent a physically meaningful propagating pattern. The estimated d.o.f. is the total number of data samples (182 days (MJASO) x 22 years = 4004) divided by the timescale of the oscillation (~ 50 days).

The leading two inseparable EOFs explain about 16% (8.8% and 7.1%) of the intraseasonal (25–80-day) variance in this domain. The two modes closely resemble the leading two OLR EOFs found by Lau and Chan (1986) for the 1975 to 1982 summers. The maximum correlation between the two principal component timeseries is 0.66 at a 9–10 day lag (Fig. 4.3b), indicating an oscillation period of around 36–40 days. The leading two EOFs together describe a propagating mode that appears to capture the low frequency convective signature that is unique to the northern summer ISO. The ISO signature, described in detail in Section 3.3, begins with equatorial convection in the central equatorial Indian Ocean (EOF1) which propagates to the east. Associated with the eastward propagating convection along the equator is a northwestward tilting band of convection (EOF2) that is responsible for the northward propagation that is observed along individual meridians across the Indian Ocean basin. One can reconstruct an OLR timeseries based on the leading

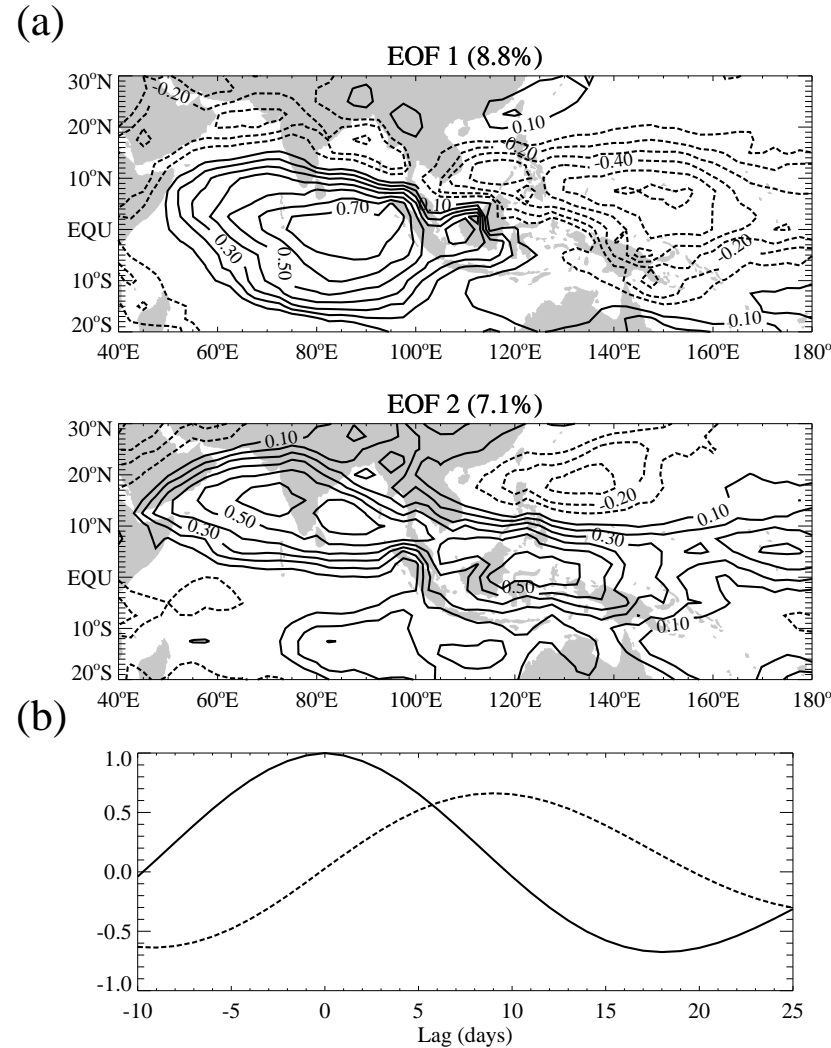


Figure 4.3. (a) Leading two EOF loading vectors of extended northern summer 25–80-day filtered OLR. Extended northern summer is May to October. EOFs calculated from data in limited domain shown. Contours are every 0.1 with the zero contour omitted. (b) Lagged cross-correlation of principal component timeseries. EOF mode 1 with itself (solid line), EOF mode 1 with EOF mode 2 (dashed line).

two EOFs by matrix multiplying the eigenvectors with their respective principal component timeseries; that is,

$$OLR_{EOF}(s, t) = \sum_{j=1}^2 e_j(s)a_j(t) \quad (4.4)$$

where e_j is the eigenvectors and a_j is the principal component timeseries and OLR_{EOF} is the reconstructed OLR timeseries.

A primary drawback of EOF analysis is that the retrieved eigenmodes can be sensitive to the choice of subdomain. To counter this limitation, the results of an EOF analysis can be rotated such that the principal component timeseries remain temporally orthogonal while the spatial orthogonality constraint of the EOF modes is relaxed. The advantages of rotation are that the results are stable to the choice of subdomain and that each EOF mode is highly correlated with timeseries in only a few geographical regions; thus, each grid point timeseries is described by as few as possible modes (Richman 1986).

The leading three modes of a rotated EOF analysis of extended summer OLR_{25-80} over the same subdomain described above are shown in Fig. 4.4a. The results are similar to those shown in Fig. 4.3 except that here the first *three* rotated EOF modes are found to be inseparable. Together, the leading three rotated EOFs describe basically the same propagating mode as that described by the leading two unrotated EOFs. The total variance explained by the three leading rotated EOF modes is only slightly greater (17%) than that explained by the leading two unrotated EOF modes (16%). Furthermore, individual grid point timeseries of OLR reconstructed from the leading two EOF modes and the leading three rotated EOF modes correlate at greater than 0.94 throughout the core Indian monsoon region. The similarity between the results of the unrotated and the more stable rotated EOF analyses suggests that the unrotated EOF analysis adequately extracts the northern

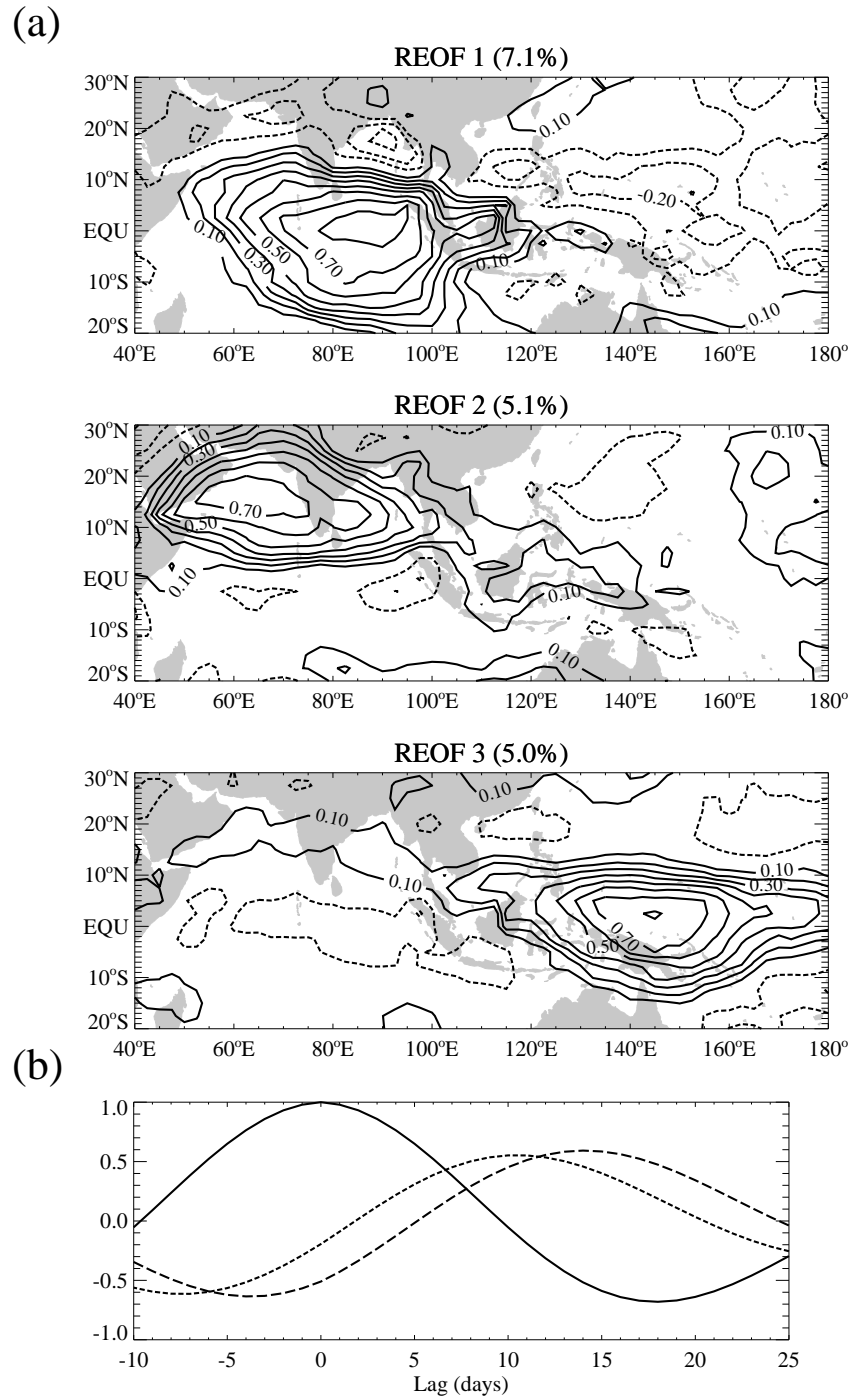


Figure 4.4. (a) Leading three rotated EOF loading vectors of northern summer 25–80-day filtered OLR. Contours are every 0.1 with the zero contour omitted. (b) Lagged cross-correlation of rotated principal component timeseries. Rotated EOF mode 1 with itself (solid line), rotated EOF mode 1 with EOF mode 2 (short dashed line), rotated EOF mode 1 with rotated EOF mode 3 (long dashed line).

summer ISO convective signature. For the remainder of this chapter, the results presented make use of OLR reconstructed from the simpler unrotated EOF modes. However, all the primary results were tested with OLR reconstructed from the rotated EOF modes. No significant differences were observed, indicating that both EOF analyses capture essentially the same predominant characteristics of the summertime ISO.

It is relevant to note that restricting the EOF and rotated EOF analyses to boreal summer is required to extract the modes shown here. When data from the entire year is analyzed, the dominant intraseasonal mode is the strictly eastward propagating ISO that is encountered during boreal winter and spring (Lau and Chan 1988; Zhang and Hendon 1997).

The variance of the two filtered datasets, OLR_{EOF} and OLR_{25-80e} , is assessed using wavelet analysis (for details on wavelet analysis, see Torrence and Compo 1998). At each grid point and for each extended summer season, the wavelet variance spectrum is calculated from 184-day (May to October) filtered OLR time-series (OLR_{EOF} or OLR_{25-80e}) using a Morlet wavelet basis. The individual wavelet variance spectra are averaged over all 45 grid points within a core Indian monsoon region ($70^{\circ}\text{--}90^{\circ}\text{E}$, $10^{\circ}\text{--}20^{\circ}\text{N}$) and over the 22 extended summers included in this study to produce the composite wavelet variance spectra shown in Figs. 4.5 and 4.6.

The composite wavelet variance spectrum of OLR_{EOF} (Fig. 4.5a) exhibits maximum variance in early June at periods just under 40 days. The wavelet variance remains high throughout the summer monsoon season before dipping noticeably in October. The mean oscillation period slowly increases from near 37 days at the

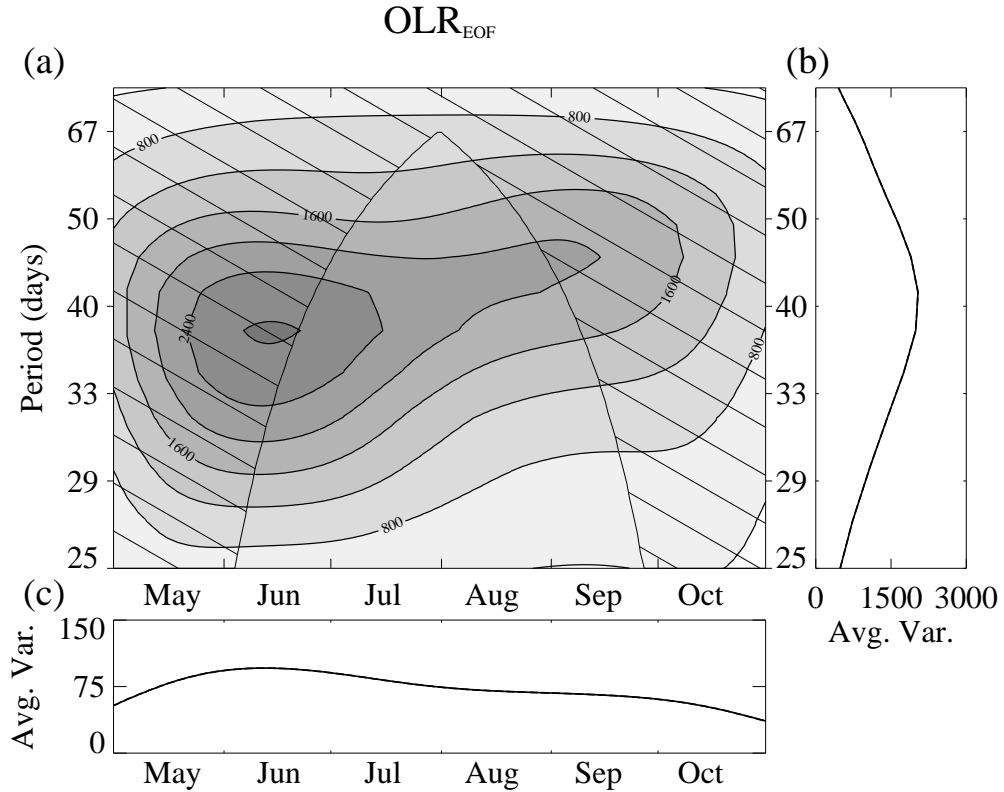


Figure 4.5. Wavelet analysis of reconstructed OLR_{EOF}. Wavelet analyses are completed on 184-day (May–October) OLR_{EOF} timeseries at each grid point included in 70°–90°E, 10°–20°N box. The 45 (9 longitudes x 5 latitudes) wavelet spectra are averaged to generate an areal averaged wavelet spectrum for each year. The 22 individual wavelet spectra from 1975–1997, excluding 1978, are averaged to form an ensemble wavelet variance spectrum. (a) Ensemble average wavelet variance spectrum. Contour levels are every 400 W² m⁻⁴ from white to dark grey. Area filled with slanted lines indicates times and periods which are not outside the cone of influence (see Torrence and Compo 1998)). Wavelet variance at those times and periods may be influenced by edge effects. (b) Frequency spectrum generated by averaging (a) over the June–September period. (c) Scale-averaged wavelet variance over 25–80-day period band.

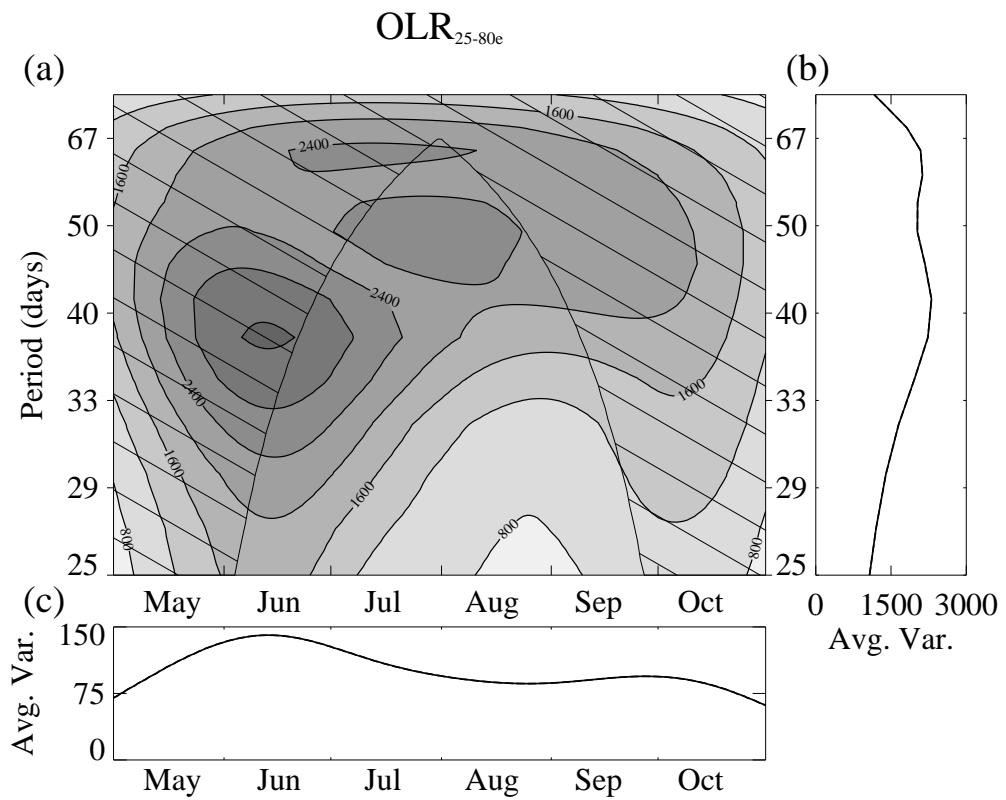


Figure 4.6: Same as Fig. 4.5 except wavelet analysis of OLR_{25-80e} .

beginning of the monsoon season to around 46 days by the end of the season. Figure 4.5b shows the mean frequency spectrum generated by averaging the wavelet variance spectrum over the June to September period only. The frequency spectrum exhibits a peak at 40 days. The composite wavelet variance timeseries is derived by computing a weighted average of the wavelet variance spectrum. The use of wavelet derived variance is chosen in lieu of squared-bandpass variance because, for a wavelet derived variance estimate, short timescale fluctuations are analyzed with a short window and long timescale fluctuations are analyzed with a long window, thus providing a more accurate estimate of the total variance within the period band. The composite wavelet variance timeseries (Fig. 4.5c) reflects the visible characteristics of the total wavelet spectrum, with the highest variance encountered at the beginning of the monsoon season followed by a steady mean variance through the rest of the monsoon season before a significant drop in ISO variance during October. The rise in mean ISO variance in May and the fall in mean ISO variance during October reflects the seasonal cycle of the regional influence of the ISO. During the remainder of the year, intraseasonal OLR variance is substantially reduced at Indian subcontinent latitudes as the ISO is located primarily along the equator (Madden 1986; Hendon and Salby 1994).

The composite wavelet spectrum of OLR_{25-80e} (Fig. 4.6) exhibits similar features to that of OLR_{EOF} with maximum variance in June at a 40 day period followed by reduced, but still high, wavelet variance during July through September at 40–50-day periods. A secondary peak in the frequency spectrum occurs at around 60-day periods (Fig. 4.6). It is not clear what is responsible for this low-frequency peak. It is entirely possible that the low-frequency peak is a statistical

artifact, especially since most of the wavelet variance at this scale is not outside the cone-of-influence introduced by the boundaries.

The seasonal mean variance distributions of OLR_{25-80}^2 , OLR_{EOF}^2 , and OLR_{25-80e}^2 are shown in Fig. 4.7. The variance distributions are determined by calculating the wavelet variance spectrum at each grid point and averaging the scale-averaged wavelet variance timeseries, such as the ones shown in Figs. 4.5c and 4.6c, over the June to September period. Both the OLR_{EOF}^2 and OLR_{25-80e}^2 represent roughly 1/3 to 1/2 of the total intraseasonal OLR variance in the Indian monsoon region. The OLR_{EOF} variance misses entirely the peak in total intraseasonal variance over the South China and Philippine Seas but closely mirrors the total intraseasonal variance distribution within the Indian monsoon domain.

4.3 Monsoon Indices and Monsoon-ENSO Relationships

4.3.1 Monsoon Indices The necessity of an index that represents interannual Indian monsoon variability is well appreciated. Unfortunately, the definition of such an index is not entirely straightforward (Wang and Fan 1999) which has led to the development of a variety of indices that all aim to gauge various facets of the seasonal strength of the monsoon:

- all-India rainfall index (AIRI) which is based on a June to September weighted average of 306 well distributed rain-gauge stations across India (Parthasarathy *et al.* 1992; Parthasarathy *et al.* 1994),
- the zonal monsoon circulation index (M) which is defined as the difference between the lower level (850-mb) and the upper level (200-mb) zonal winds averaged over the South Asian region, $40^\circ\text{--}110^\circ\text{E}$, $0^\circ\text{--}20^\circ\text{N}$ (Webster and Yang 1992), and

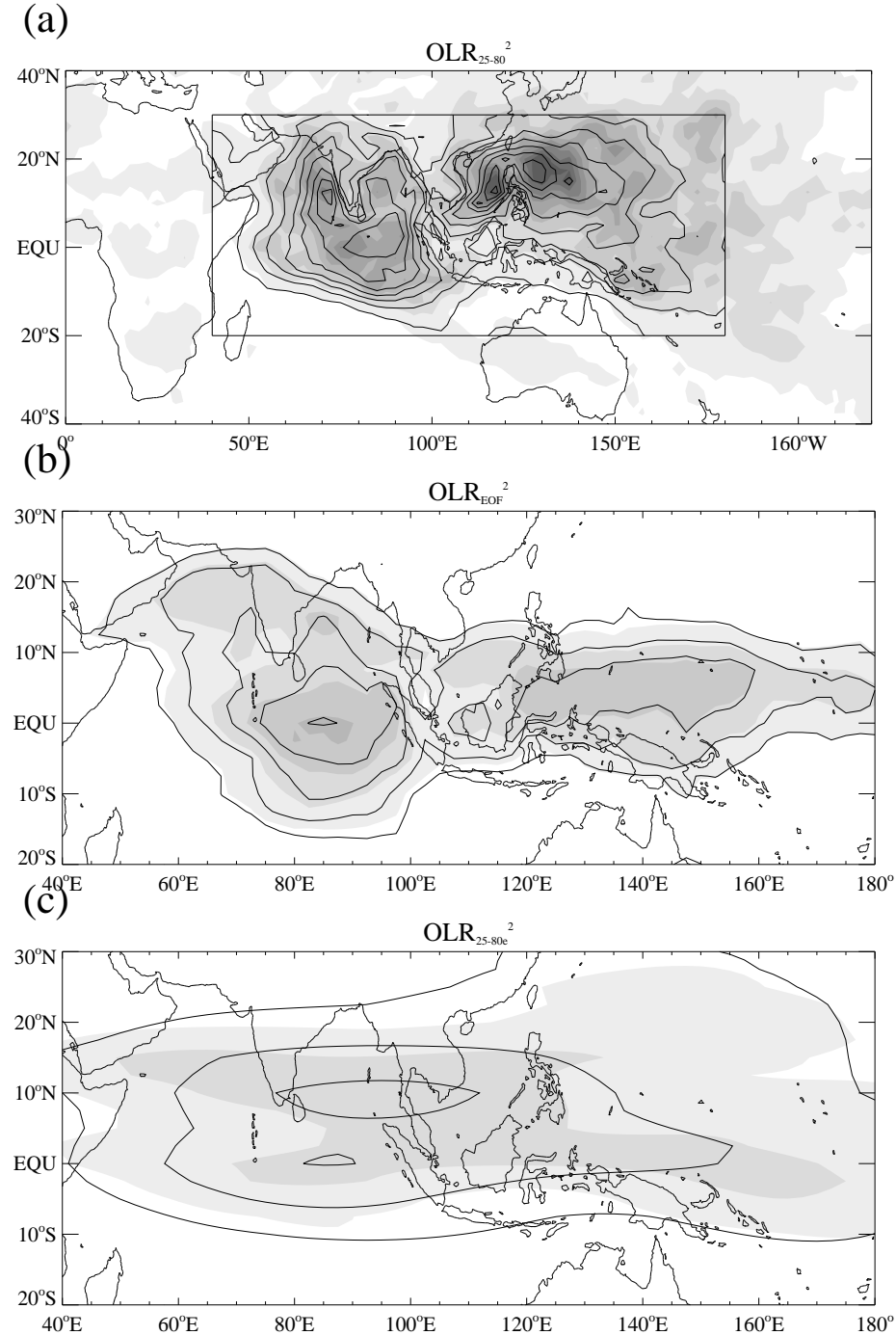


Figure 4.7. Variance maps for (a) 25–80-day filtered OLR, (b) OLR_{EOF} , and (c) OLR_{25-80e} averaged June to September 1975–1997. The contour interval is $50 \text{ W}^2 \text{ m}^{-4}$. The respective interannual standard deviations of variance are shaded with contour intervals of $25 \text{ W}^2 \text{ m}^{-4}$. Box in (a) shows domain on which EOF analysis of intraseasonal OLR is completed.

- the monsoon Hadley (MH) index which is defined as the difference between the lower level (850-mb) and the upper level (200-mb) meridional winds averaged over the same South Asian region (Goswami *et al.* 1999).

Here, the M and MH indices are determined using the NCEP/NCAR reanalysis data for the upper and lower level winds (Kalnay *et al.* 1996). Both vertical shear indices are designed to reflect the interannual variability of the broad-scale monsoon. Such a broad-scale monsoon index is desirable because the maximum monsoonal precipitation, and presumably the maximum heating, does not actually occur over India, but instead is located in the Bay of Bengal. A reasonable question to ask is whether or not a large AIRI value corresponds to a large broad-scale monsoon strength index value. Figure 4.8 shows the regression of seasonal mean OLR onto the AIRI. High anti-correlations and low regressed OLR values are seen across India and the Arabian Sea and even over portions of east Africa (for discussion on relationship between AIRI and East African rainfall, see Camberlin 1997). However, there appears to be no significant interannual relationship between the AIRI and seasonal mean OLR over the Bay of Bengal. That is, the seasonal mean precipitation over India seems to vary independently of precipitation over the Bay of Bengal. The reason for such independent variability is not clear and will be the emphasis of a future study. Nevertheless, the regression results highlight the importance of treating the interannual variability of the two regions independently; therefore, with this result in mind, three additional measures of the monsoon are calculated based on seasonal mean OLR:

- OLR_{IM} , which is the seasonal mean OLR averaged over the core Indian monsoon region, $70^{\circ}\text{--}100^{\circ}\text{E}$, $10^{\circ}\text{--}20^{\circ}\text{N}$,

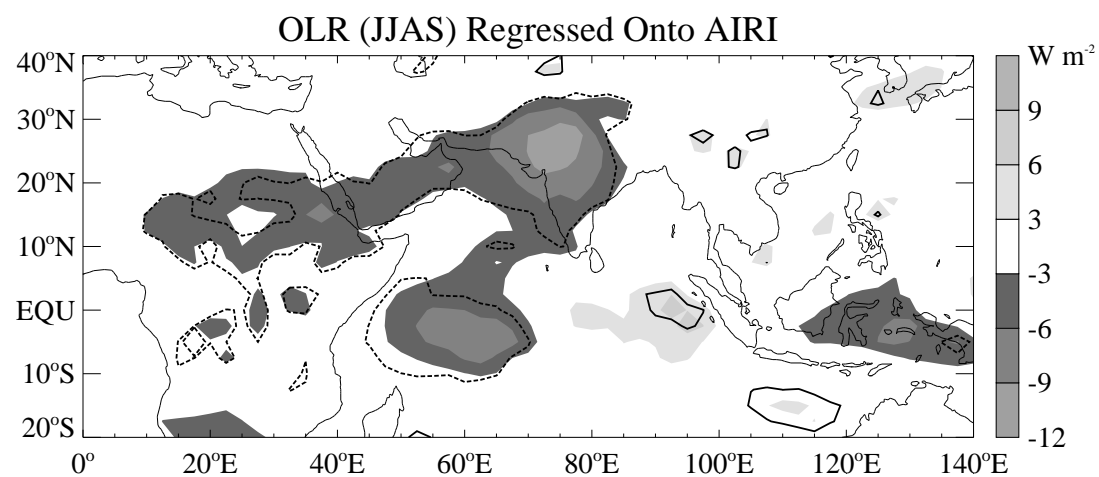


Figure 4.8. Regression of June-September mean OLR onto AIRI for the 22-years 1975–1997 (excluding 1978). Dark lines indicate where the regression correlation coefficients exceed the 95% significance level based on 22 d.o.f. (± 0.36).

- $\text{OLR}_{\text{India}}$, which is the seasonal mean OLR averaged only over Indian land-mass grid points, and
- OLR_{BB} , which is the seasonal mean OLR averaged only over Bay of Bengal grid points.

The interannual relationships between the monsoon indices are summarized in Table 4.1 which lists the correlations amongst all the indices. As anticipated by the regression results shown in Fig. 4.8, the AIRI does not correlate strongly with OLR_{BB} , but does correlate well with $\text{OLR}_{\text{India}}$. Interestingly, the AIRI and $\text{OLR}_{\text{India}}$ themselves do not correlate perfectly (0.70). For the sake of simplicity and to provide a "best estimate" of interannual Indian monsoon rainfall variability a combined monsoon index is introduced that is defined as

$$\text{AIRI-OLR}_{\text{India}} = \frac{\text{AIRI} - \overline{\text{AIRI}}}{\sigma_{\text{AIRI}}} - \frac{\text{OLR}_{\text{India}} - \overline{\text{OLR}_{\text{India}}}}{\sigma_{\text{OLR}_{\text{India}}}} \quad (4.5)$$

where the minus sign in front of the second term on the right is due to inverse relationship between rainfall and OLR. Theoretically, since M and MH are designed to reflect the broad-scale monsoon variability, they should correlate strongly with the total monsoon OLR index, OLR_{IM} , but the correlations are relatively weak at 0.35 and 0.23, respectively. In fact, both indices surprisingly correlate better with $\text{OLR}_{\text{India}}$ than OLR_{IM} . There has been some speculation that the monsoon circulation indices suffer from a too weak divergent wind in the NCEP/NCAR reanalysis product (Webster and Tomas, personal communication).

4.3.2 Monsoon-ENSO Relationships The state of ENSO is evaluated here using the Niño3 SST index, which is calculated by averaging monthly Reynolds SST over the domain 5°S – 5°N , 150° – 90°W . Over the 22 years considered in this study, the simultaneous correlations between JJAS Niño3 SST and the AIRI,

Table 4.1. Correlations between seasonal Indian monsoon indices over 22 years (1975–1997, excluding 1978). For all correlations, a positive correlation value indicates a positive relationship between the two measures of monsoon strength.

Monsoon Index	AIRI	OLR_{IM}	OLR_{India}	OLR_{BB}	M	MH
AIRI	—					
OLR_{IM}	0.23	—				
OLR_{India}	0.70	0.71	—			
OLR_{BB}	0.04	0.93	0.52	—		
M	0.27	0.35	0.58	0.20	—	
MH	0.50	0.23	0.59	0.27	0.22	—

$\text{OLR}_{\text{India}}$, OLR_{IM} , and OLR_{BB} are -0.32 , 0.44 , 0.18 , and 0.02 , respectively. Correlations are slightly greater by about 0.1 if the subsequent DJF Niño3 SST is used to represent ENSO (the larger correlations are due to wintertime peak in evolution of ENSO events, (Torrence and Webster 1999)). Historically, the inverse correlation between ENSO and Indian rainfall has been stronger and the relatively weak correlations over the 22 year record considered here may reflect observations that the monsoon-ENSO relationship is weakening in the 1990's (Goswami *et al.* 1999). In particular, despite the near record strength of the 1997 El Niño , the Indian monsoon rainfall was close to normal (Webster and Palmer 1997).

4.4 Interannual Variations of ISO Activity

4.4.1 Changes in ISO Characteristics Indices that capture the year-to-year variations of summertime ISO activity in the Indian monsoon region are determined by averaging an individual season's wavelet derived variance timeseries (e.g. Fig. 4.5c except for a single extended summer, not the ensemble mean) across the June to September period. The seasonal estimates of the two ISO activity indices, $[\text{OLR}_{\text{EOF}}^2]$ and $[\text{OLR}_{25-80e}^2]$, are shown in Fig. 4.9. The two ISO activity indices correlate with each other at 0.83 , indicating that they capture largely similar interannual fluctuations of ISO activity.

The first question to ask is whether or not the objectively defined $[\text{OLR}_{\text{EOF}}^2]$ and $[\text{OLR}_{25-80e}^2]$ ISO activity indices reasonably reflect observed interannual summertime ISO activity fluctuations. A visual inspection of time-latitude OLR diagrams indicates that seasons of high (low) ISO activity as defined by the wavelet derived indices are (are not) characterized by regular northward propagation of convection. Furthermore, a linear regression of the total seasonal mean OLR_{25-80} variance onto $[\text{OLR}_{\text{EOF}}^2]$ (Fig. 4.10) shows that enhanced ISO activity in the Indian

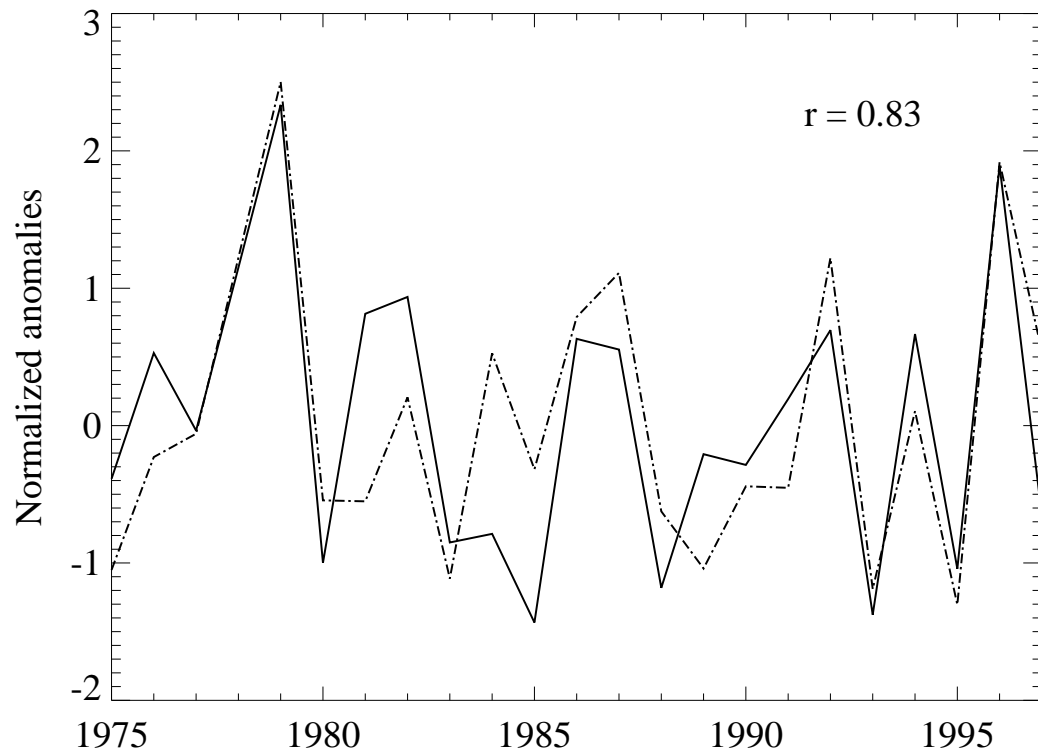


Figure 4.9. Seasonally averaged ISO activity indices for JJAS. Solid line is ISO activity index based on variance of OLR reconstructed from EOF1 and EOF2. Dashed line is index based on seasonal variance of OLR filtered to 25–80-days and eastward wavenumbers 1 through 6. Both indices represent spatially averaged variance over the core Indian monsoon region 70° – 90° E, 10° – 20° N.

monsoon region coincides with enhanced intraseasonal variance across the north Indian Ocean basin as well as areas to the north of the equator in the western Pacific Ocean. The area of enhanced intraseasonal convective variance largely mirrors the climatological OLR_{EOF} variance shown in Fig. 4.7b, indicating that interannual variations of the [OLR_{EOF}²] index reflect interannual variations of the entire summertime ISO system, which includes both eastward propagation along the equator and northward propagation onto the Indian subcontinent.

A characteristic ISO period can be deduced by averaging the seasonal wavelet variance spectrum from June to September (e.g., Fig. 4.5b except for single season) and identifying the period exhibiting maximum variance. The characteristic periods, determined by this method, vary widely from a low of 27 days to a high of 63 days for both ISO activity indices. The true spread of ISO periods may not be as broad because, during seasons when the [OLR_{EOF}²] and [OLR_{25–80e}²] indices are low, a characteristic period cannot be clearly distinguished because the average frequency spectrum is weak and nearly flat (not shown). During seasons when ISO activity is strong, and therefore a characteristic ISO period is readily identified, the characteristic period range is limited to between 34 and 45 days for both indices. The correlation between the characteristic period and the ISO activity index during strong ISO activity seasons is only 0.14 for [OLR_{EOF}²] and –0.01 for [OLR_{25–80e}²]. The low correlations imply that the period of oscillation is not a decisive factor in determining the amplitude of ISO activity.

In contrast, correlations between ISO activity indices and the number of discrete active and break periods are 0.61 and 0.58 for [OLR_{EOF}²] and [OLR_{25–80e}²]. The active and break episodes are defined, relative to the core Indian monsoon region, as minimums and maximums of OLR_{EOF} and OLR_{25–80e} that are greater

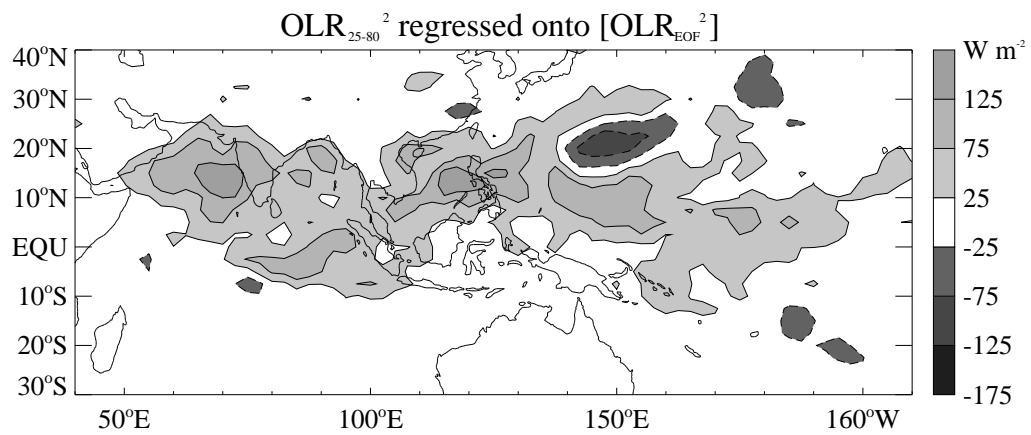


Figure 4.10. Regression of June-September mean OLR_{25-80}^2 onto $[\text{OLR}_{\text{EOF}}^2]$ for the 22-years 1975–1997 (excluding 1978). OLR_{25-80}^2 is shown as anomalies from the seasonal mean OLR_{25-80}^2 distribution for a 1.5σ anomaly of $[\text{OLR}_{\text{EOF}}^2]$. Regression onto $[\text{OLR}_{25-80e}^2]$ is similar due to high mutual correlation with $[\text{OLR}_{\text{EOF}}^2]$.

than one-standard-deviation (σ) from the long term mean. By this definition, the number of discrete active and break events that occur each season ranges from 1 to 6 per season.

The relationship between ISO activity and precipitation is examined in more detail by utilizing a daily precipitation dataset. This precipitation dataset spans the years 1979–1995, a 17 year subset of the OLR data, and merges daily station data over land with Microwave Sounding Unit (MSU) data over the oceans. Due to the non-Gaussian distribution of precipitation, a more robust method of identifying the $\pm 1\sigma$ estimates is required to identify "active" and "break" precipitation days. The upper and lower one-standard-deviations are defined, as in Shea and Sontakke (1995), by first sorting the daily precipitation estimates from the entire 17 year summer precipitation record (96 summer days \times 17 years = 1632 total days) into ascending order. The 1/6th and 5/6th sextiles are then defined as

$$\hat{X}_{\frac{1}{6}} = z\left(\frac{N}{6}\right) \quad \text{and} \quad \hat{X}_{\frac{5}{6}} = z\left(\frac{5N}{6}\right) \quad (4.6)$$

where N is the total number of days (1632) and $z(n)$ is the precipitation timeseries after sorting into ascending order. Days in which precipitation values fall below $\hat{X}_{\frac{1}{6}}$ and above $\hat{X}_{\frac{5}{6}}$ are defined as "break" and "active" days, respectively. The 96 day precipitation timeseries begin at the relatively late date of June 15 of each year to eliminate the influence of monsoon onset on the precipitation distribution.

One would anticipate that a season of strong ISO activity would include both more active and more break days than during a season of comparatively weak ISO activity. Figure 4.11a shows the average number of days in which precipitation over central India falls into each sextile for the top five ISO activity years as defined by the $[\text{OLR}_{EOF^2}]$ index. The anticipated normal number of days in each sextile would be 16 (96 days in season divided by 6 sextiles). During strong ISO activity

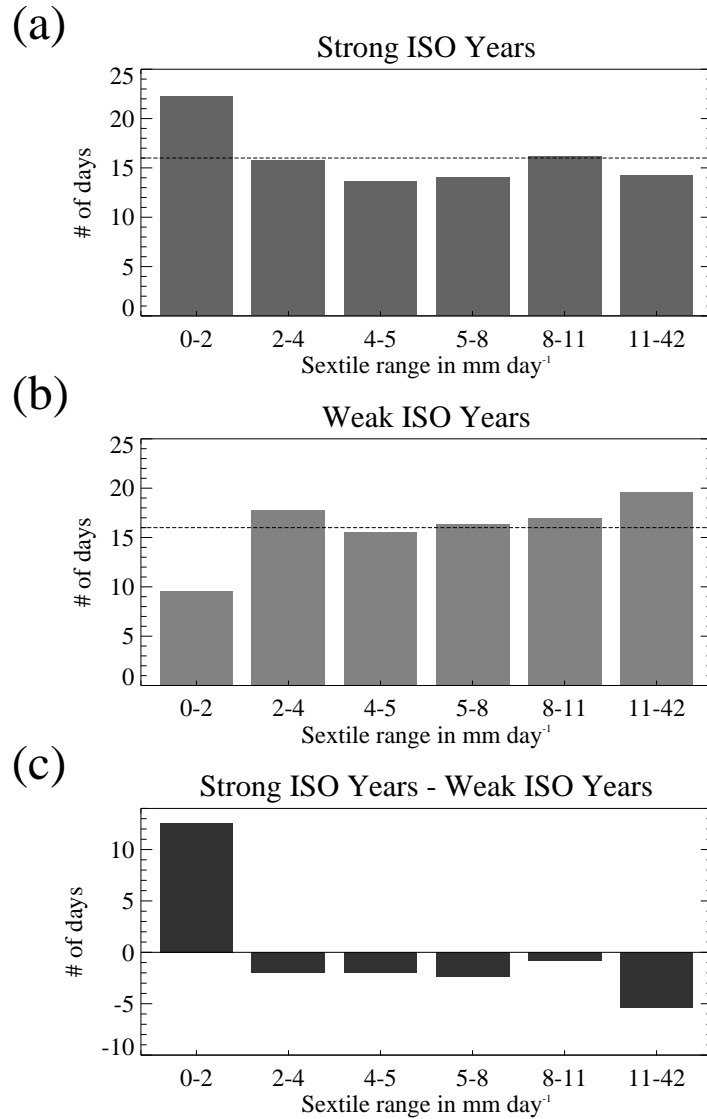


Figure 4.11. Composite histogram of number of days per season in which the daily area-averaged precipitation falls into each of six sextiles during (a) top five ISO activity years (1979, 1982, 1986, 1987, 1992), (b) bottom five ISO activity years (1983, 1988, 1989, 1993, 1995), and (c) top five ISO activity seasons minus bottom five ISO activity seasons. Only years when precipitation data is available are considered (1979–1995). For each season, 96 daily precipitation estimates, starting June 15 and averaged over peninsular India (75° – 80° E, 10° – 20° N), are taken yielding a total of $96 \times 17 = 1632$ days. The precipitation values are sorted according to magnitude and cutoff values are defined for each of the six sixths. The number of days per sextile is the average number of days, e.g. for the strong ISO activity seasons, that the daily precipitation falls into a particular sextile. The expected normal number of days in any individual sextile is 16 (96/6).

years, there are approximately 22 break days per season, 6 more than would be expected during a normal year. Conversely, Fig. 4.11b shows the composite sextile histogram for the five weakest ISO activity years. During weak ISO activity seasons, seasons when presumably there are not large scale swings between active and break periods over India, the average number of break days is only 9.5. The composite differences are shown in Fig. 4.11c. On average, there are 12.5 more break days during a strong ISO activity season relative to a weak one. Interestingly, the number of active days actually declines during a strong ISO activity season compared to a weak ISO activity season which suggests that the entire precipitation distribution shifts towards smaller daily precipitation values during strong ISO activity seasons, and vice versa.

The same analysis done for precipitation over the central Bay of Bengal is shown in Fig. 4.12. While the number of break days is marginally greater during strong ISO activity seasons, the change in precipitation distribution is weaker over the ocean relative to that over land.

The results of this section are briefly summarized here:

- The year-to-year variations of summertime ISO activity appear to be reasonably captured by the $[\text{OLR}_{EOF}^2]$ and $[\text{OLR}_{25-80e}^2]$ indices. The indices, defined by variance changes in the core Indian monsoon region, reflect interannual variability of the entire summertime ISO system.
- The fluctuations in the ISO activity indices are not closely linked to changes in ISO period, but instead reflect the number of discrete active and break events that occur within each season.

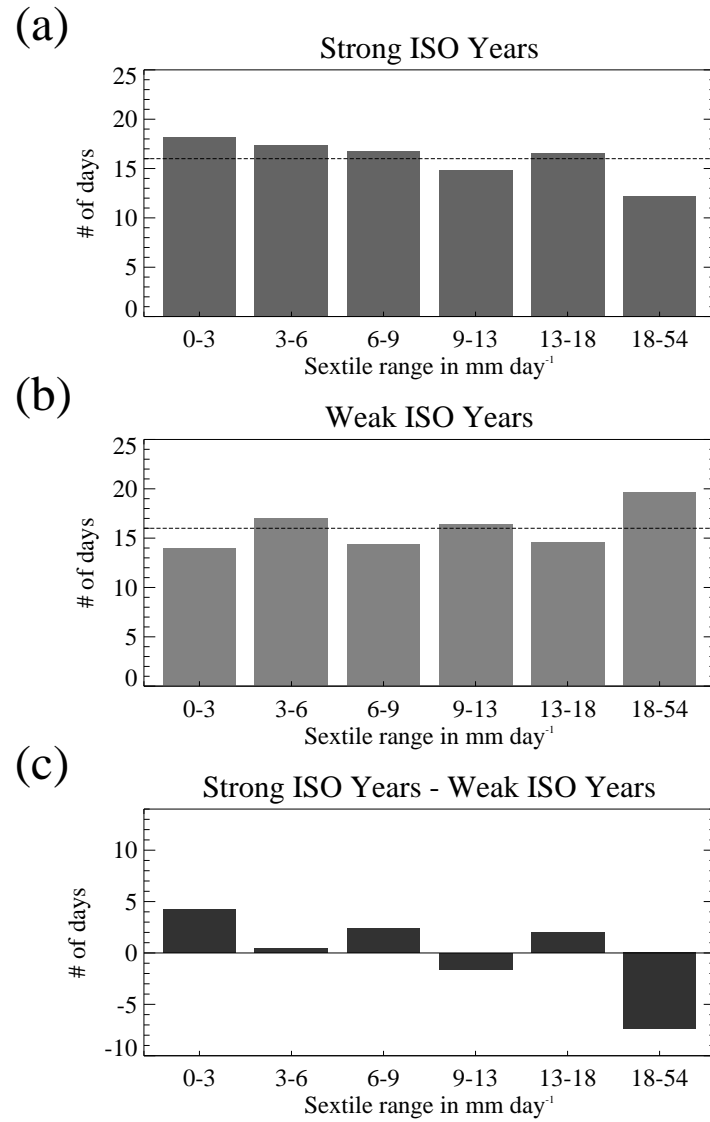


Figure 4.12. Same as Fig. 4.11 except precipitation averaged over central Bay of Bengal ($85^{\circ}\text{--}90^{\circ}\text{E}$, $12^{\circ}\text{--}17^{\circ}\text{N}$).

- Seasons of strong ISO activity, particularly over land, exhibit a substantial increase in the number of break precipitation days relative to seasons of weak ISO activity.

4.4.2 Relation to Interannual SST Variability

4.4.3 ENSO Because of the established inverse relationship between ENSO and the Indian monsoon, it is important to examine the associations between ISO activity and ENSO before one can comment on the relationship between ISO activity and the Indian monsoon. The simultaneous correlations between JJAS Niño3 SST and $[\text{OLR}_{EOF}^2]$ and $[\text{OLR}_{25-80e}^2]$ are weakly positive at 0.16 and 0.22, respectively. Hendon *et al.* (1999) found that the wintertime ISO activity is essentially uncorrelated with DJF Niño3 SST, although notable reductions in wintertime ISO activity are observed during the two strongest recent ENSO events (1982-83, 1997-98). Of the four warmest JJAS Niño3 SST years included in this study, two exhibit above normal $[\text{OLR}_{EOF}^2]$ levels (1982, 1987) and two exhibit below normal $[\text{OLR}_{EOF}^2]$ levels (1983, 1997). In contrast, of the coolest four JJAS Niño3 SST years, three exhibit below normal $[\text{OLR}_{EOF}^2]$ (1975, 1985, 1988) while only one exhibits above normal $[\text{OLR}_{EOF}^2]$ (1981).

Composites of the OLR_{EOF} wavelet spectra for the four warmest and four coolest JJAS Niño3 SST years are shown in Figs. 4.13 and 4.14. For the warm JJAS Niño3 SST composite (Fig. 4.13), the OLR_{EOF} variance tends to be above normal at the beginning of the monsoon season in May through July and below normal for the remainder of the season such that the total summertime variance is near normal. For the cool JJAS Niño3 SST composite (Fig. 4.14) the early part of the monsoon season is characterized by weaker than normal ISO activity while the remainder of the season exhibits near normal ISO activity. It is important to note

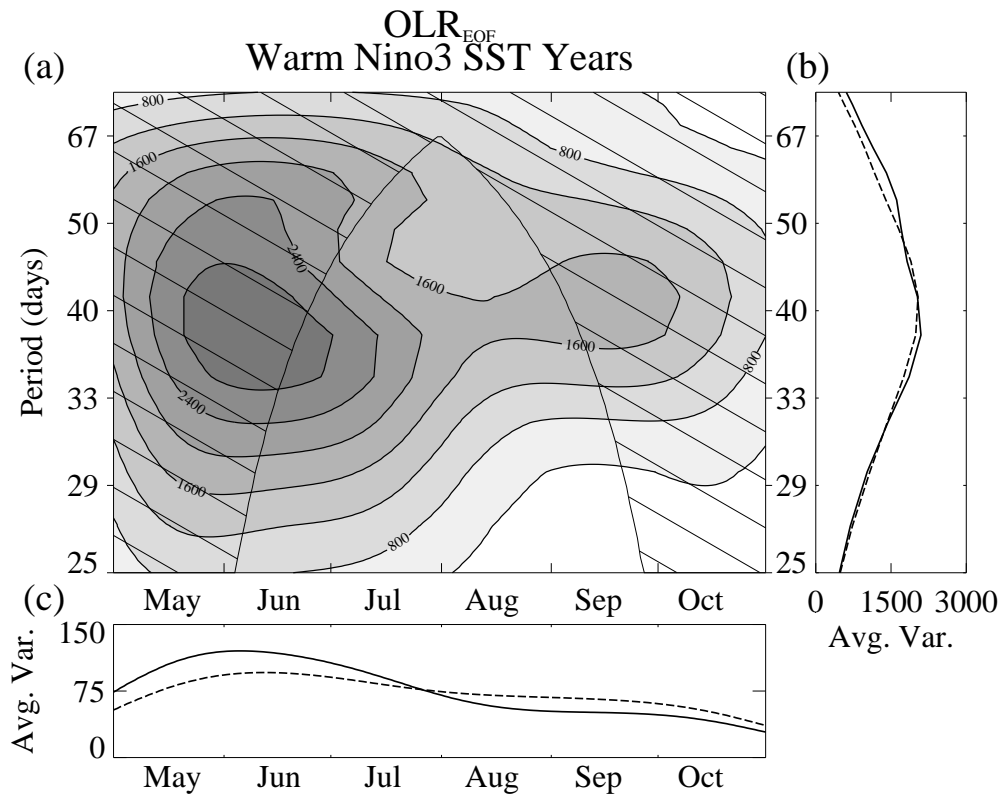


Figure 4.13. Same as Fig. 4.5 except composite of four warmest JJAS Niño3 SST years (1982, 1983, 1987, 1997). Dashed lines show mean variance from all-years composite.

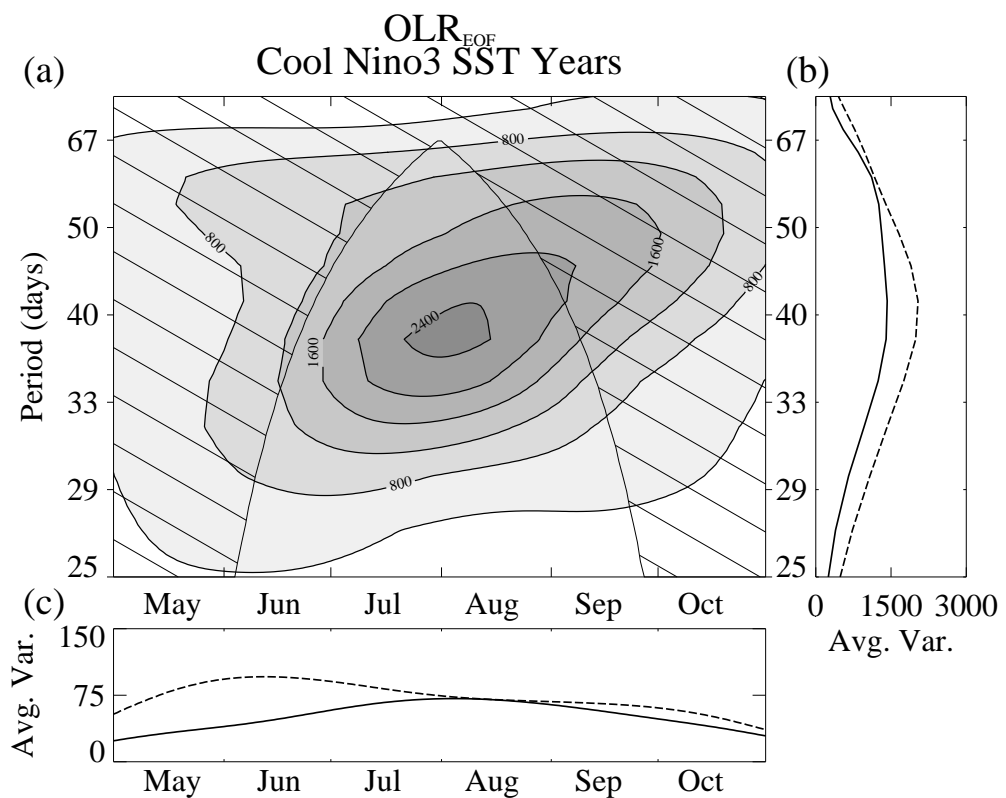


Figure 4.14. Same as Fig. 4.5 except composite of four coolest JJAS Niño3 SST years (1975, 1981, 1985, 1988).

that the composites shown in Figs. 4.13 and 4.14 include only four seasons each; consequently, the significance of the results must be evaluated with this limitation in mind. Nevertheless, the modest positive correlation between mean seasonal ISO activity and ENSO appears due to changes in early monsoon season ISO activity associated with the state of ENSO. Correlations between JJAS Niño3 SST and ISO activity are 0.38 ($[OLR_{EOF}^2]$) and 0.35 ($[OLR_{25-80e}^2]$) for the first two months of the monsoon season and only -0.03 and 0.02 for the latter two months of the season.

The mean frequency spectra of the OLR_{EOF} wavelet spectra composites for warm and cool JJAS Niño3 SST are shown in Figs. 4.13b and 4.14b. No distinguishable shift in ISO period can be discerned during either ENSO phase. The lack of a period shift associated with the phase of ENSO runs counter to the model results of Krishnan and Kasture (1996), in which they found that warm ENSO years are characterized by slower oscillations. However, Krishnan and Kasture also found that warm ENSO seasons exhibit more regular ISO behavior, a result that is weakly supported by the analysis completed here.

Hendon *et al.* (1999) found that during warm ENSO episodes, there is an eastward shift of ISO activity during winter (see also Fink and Speth 1997), but the anomalies are small compared to the standard interannual deviations. To test whether or not there is a corresponding shift in the distribution of ISO activity during summer, the total OLR_{25-80} variance and the OLR_{25-80e} variance are regressed onto JJAS Niño3 SST (not done for OLR_{EOF} because the location of variance is essentially prescribed by EOF modes). The only significant change in location of either measure of intraseasonal convection variance is an extension of variance eastward in the Pacific Ocean to about 160°W during the positive ENSO phase. Within

the Indian Ocean basin, there is no change in location or amplitude of intraseasonal convection variance with the phase of ENSO (not shown).

To summarize the preceding analysis, the phase of ENSO during northern summer does not strongly impact the amplitude or location of seasonally averaged summertime ISO activity. However, ISO activity at the beginning of the monsoon season *does* appear to be influenced by the phase of ENSO with moderately enhanced ISO activity observed during the warm ENSO phase and vice versa.

4.4.4 Other SST Variability The question remains, then, as to what is forcing the interannual variability of summertime ISO activity. To explore further the possible role of other SST anomalies, besides those associated with ENSO, the global summertime mean SST is regressed onto the $[\text{OLR}_{EOF}^2]$ and $[\text{OLR}_{25-80e}^2]$ indices (Fig. 4.15). Both regressions show virtually no coincident relationship between any tropical SST variability and ISO activity. Hence, the importance of SST boundary forcing on the level of ISO activity seems to be minimal although it remains possible that small interannual changes in SST generate large year-to-year changes in ISO activity in a nonlinear manner. If the interannual variations of ISO activity are not related to interannual SST variations then the source of the year-to-year variations in ISO activity must either be forced by land surface boundary conditions or internally generated.

4.4.5 Relation to Interannual South Asian Monsoon Variability

With indices defined for both the seasonal ISO activity and seasonal monsoon strength, it is possible to investigate the relationship between interannual variations of ISO activity and interannual fluctuations of the monsoon. Figure 4.16 is a scatter diagram of $[\text{OLR}_{EOF}^2]$ versus OLR_{India} . The two indices correlate at +0.56, which means that there is an inverse relationship between the strength of the Indian

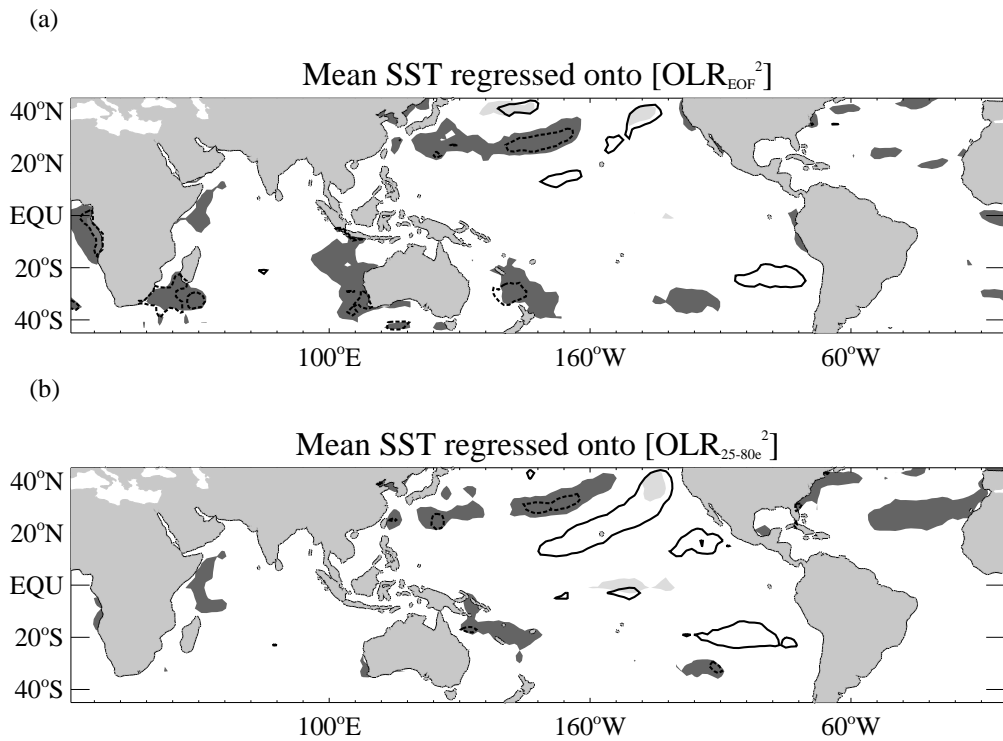


Figure 4.15. Regression of June–September anomalous SST onto (a) $[\text{OLR}_{\text{EOF}}^2]$ and (b) $[\text{OLR}_{25-80e}^2]$. Contour intervals are every 0.25°C beginning at $\pm 0.125^\circ\text{C}$. Black lines denote where correlation coefficients are significant at 95% level based on 22 d.o.f. (± 0.36).

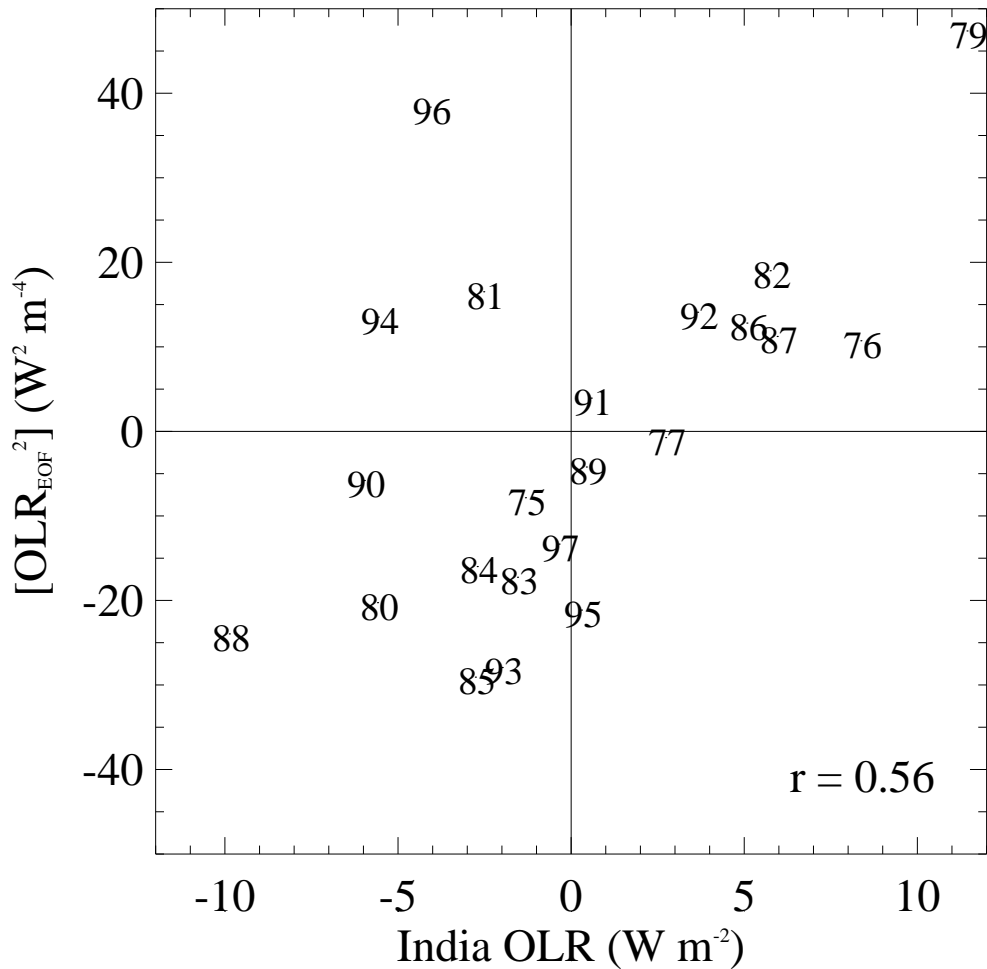


Figure 4.16. Scatter diagram of summertime $[OLR_{EOF}^2]$ versus OLR-India. Both indices are plotted as anomalies from their respective 22-year means. The correlation is 0.55 (0.70 excluding 1996). "The great tragedy of science – the slaying of a beautiful hypothesis by an ugly fact." –Thomas Huxley

monsoon and the magnitude of summertime ISO activity (recall that low $\text{OLR}_{\text{India}}$ values point to a strong monsoon). The inverse relationship is the same sign, although slightly weaker, as that found between wintertime ISO activity and Australian monsoon strength (Hendon 1999). Table 4.2 lists the correlations between the various monsoon indices and $[\text{OLR}_{\text{EOF}}^2]$ and $[\text{OLR}_{25-80e}^2]$. The correlations between $\text{OLR}_{\text{India}}$ and AIRI and the two ISO activity indices are strong (less than -0.46) and statistically significant at the 95% level in all cases. The seasonal ISO activity does not appear to be inversely correlated with precipitation over the Bay of Bengal.

While the situation is not as dire as the quotation in the caption to Fig. 4.16 suggests, the year 1996 is anomalous in that the rainfall is above normal even though it is one of the strongest ISO activity seasons over the 22-year record. A cursory examination of the 1996 rainfall timeseries did not reveal any obvious reasons for the anomaly. Nineteen ninety-six was characterized by an anomalously high number of tropical storms in the North Indian Ocean basin which could have led to the high seasonal rainfall totals. As will be shown in the next chapter, the ISO appears to modulate tropical storm activity with the majority of tropical storms forming during the convective ISO phase.

The normalized departures from average for each year between 1975 and 1997 for the $[\text{OLR}_{\text{EOF}}^2]$, $[\text{OLR}_{25-80e}^2]$, and the combined AIRI- $\text{OLR}_{\text{India}}$ indices are shown in Fig. 4.17. In general, a stronger than normal northward component of the intraseasonal oscillation corresponds to a depleted monsoon. Of the 8 seasons in which the $[\text{OLR}_{\text{EOF}}^2]$ index is substantially greater than normal ($> 0.5\sigma$), 6 are deficient Indian monsoon seasons by both indices, 2 are normal Indian monsoon seasons and only 1 is an abundant India monsoon year. Conversely, of the 7 years

Table 4.2. Correlations between seasonal ISO activity indices and Indian monsoon indices over 22 years (1975–1997, excluding 1978). ISO activity and Indian monsoon indices described in text. For all correlation values, a negative correlation indicates an inverse relationship between the interannual variability of the monsoon index and the interannual variability of the ISO activity.

Monsoon Index	JJAS ISO Activity	
	$[\text{OLR}_{EOF}^2]$	$[\text{OLR}_{25-80e}^2]$
AIRI	-0.46	-0.59
OLR_{IM}	-0.30	-0.19
OLR_{India}	-0.56	-0.46
OLR_{BB}	-0.18	-0.01
M	-0.41	-0.55
MH	-0.42	-0.37

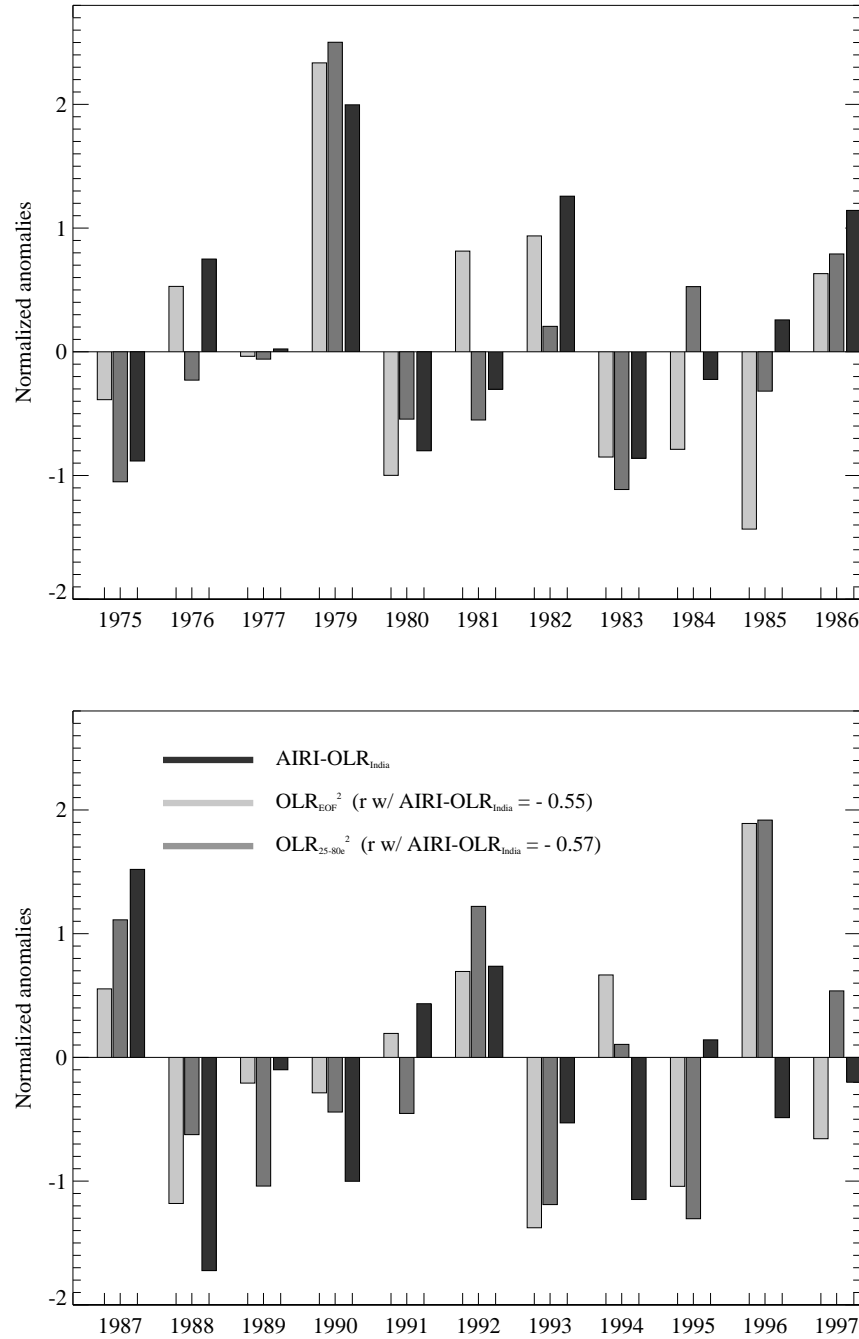


Figure 4.17. $[OLR_{EOF}^2]$, $[OLR_{25-80e}^2]$, and a combined AIRI-OLR_{India} indices expressed in units of standard deviations away from the mean. The sign of the AIRI-OLR_{India} index has been reversed such that positive (negative) AIRI-OLR_{India} index value indicates a dry (wet) Indian monsoon.

in which the $[OLR_{EOF}^2]$ index is substantially below normal ($< -0.5\sigma$), 4 are wet Indian monsoon seasons, 3 are near normal, while none are abnormally dry. Due to the high mutual correlation between the two ISO activity indices, the year-by-year breakdown is similar for the $[OLR_{25-80e}^2]$ index.

The inverse relationship between the Indian monsoon strength and ISO activity is examined further by compositing the mean OLR_{EOF} wavelet spectra for wet and dry monsoon seasons. The composite wavelet spectrum of the five wettest monsoon seasons (1975, 1980, 1983, 1988, 1990), as defined by the combined AIRI- OLR_{India} index, is shown in Fig. 4.18. The ISO variance is below normal throughout the season although more so at the beginning of the season. There is a slight indication that the period of oscillation is reduced to near 33 days during wet monsoons, but as was noted previously, the flatness of the total frequency spectrum when the wavelet variance is low precludes one from making a definitive statement about the oscillation. Out of the five wet monsoon seasons composited, two are also classified as cool JJAS Niño3 SST years. A separate composite (not shown), consisting solely of the three wettest monsoon years that are not also cool JJAS Niño3 SST years, exhibits the same general characteristics as that shown in Fig. 4.18.

The composite OLR_{EOF} wavelet spectrum of the five driest monsoon seasons (1976, 1979, 1982, 1986, 1987) is shown in Fig. 4.19. The variance is above normal, in this composite, at all times and scales. Once again, of the five driest monsoon seasons composited, two are also classified as warm JJAS Niño3 SST years. The composite wavelet spectrum of the remaining three dry monsoon years (not shown) is largely similar except that the late monsoon season variance is substantially stronger than the composite values seen in Fig. 4.19 while the early season variance is closer to normal levels.

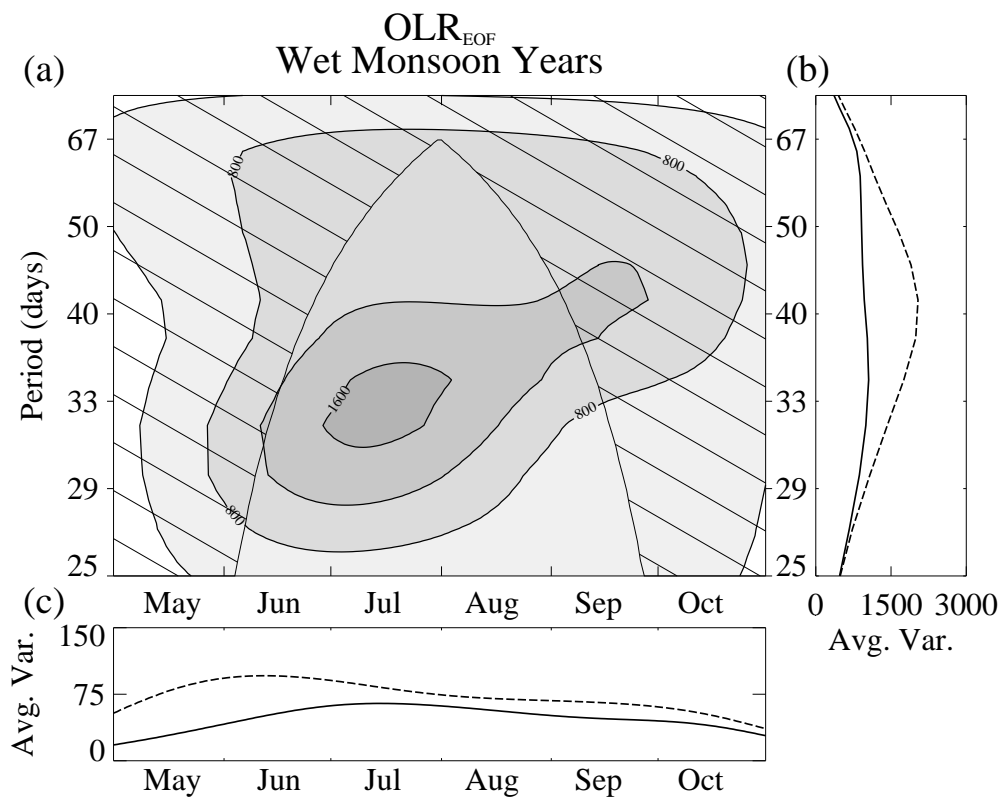


Figure 4.18. Same as Fig. 4.5 except composite of five wettest JJAS monsoon years (1975, 1980, 1983, 1988, 1990). Wet monsoon years defined by combination of AIRI and OLR-India indices.

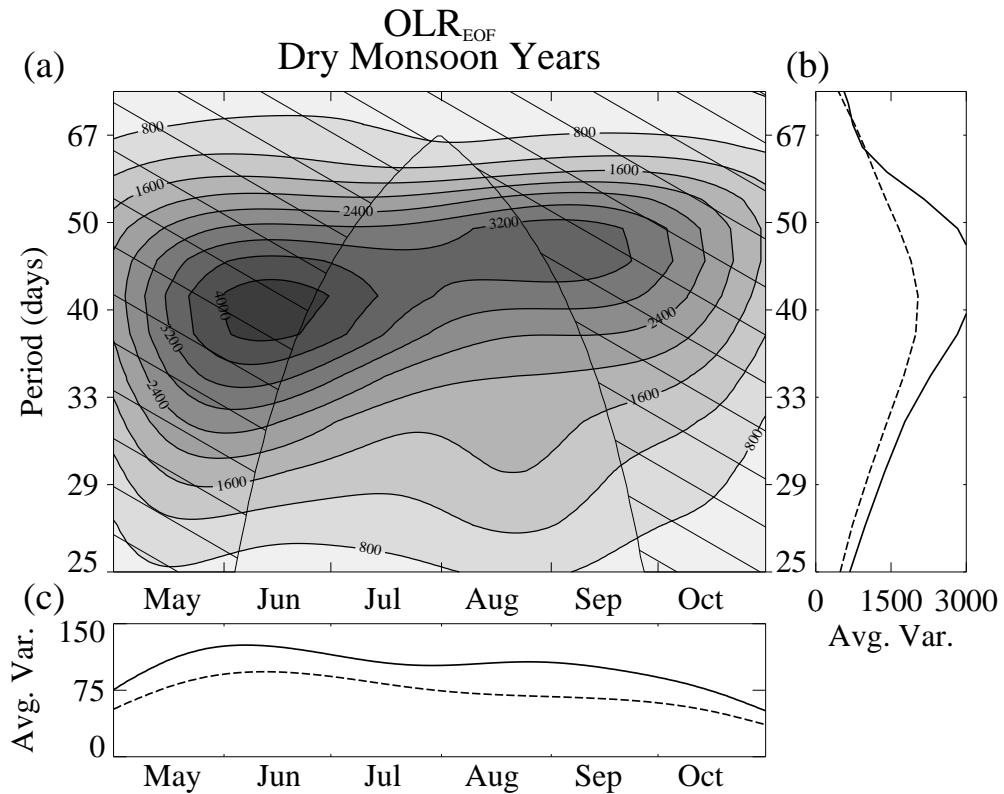


Figure 4.19. Same as Fig. 4.5 except composite of five driest JJAS monsoon years (1976, 1979, 1982, 1986, 1987). Dry monsoon years defined by combination of AIRI and OLR-India indices.

4.4.6 ISO, ENSO, and the Indian Monsoon The above results suggest that both the level of ISO activity and the state of ENSO bear some relationship to Indian monsoon strength. However, the relationship between ENSO and the ISO activity is weak, although not necessarily negligible, particularly in the early summer months. Figures 4.20a and 4.20b display the regressions of summertime mean OLR onto $[OLR_{EOF}^2]$ and JJAS Niño3 SST, respectively. OLR that is linearly dependent on JJAS Niño3 SST is removed prior to forming the regression in Fig. 4.20a. In a similar manner, OLR that is linearly dependent on $[OLR_{EOF}^2]$ is removed prior to forming the regression of mean OLR onto JJAS Niño3 SST shown in Fig. 4.20b. The anomaly patterns in Fig. 4.20b resemble the classical large scale anomaly patterns associated with ENSO including enhanced convection over the eastern Pacific Ocean and reduced convection over Indonesia, equatorial Africa, and peninsular India (e.g., Kiladis and Diaz 1989). Meanwhile, as anticipated by the inverse relationship between OLR_{India} and $[OLR_{EOF}^2]$, independent of ENSO, high ISO activity corresponds to significantly reduced convection over most of India and Bangladesh (Fig. 4.20a). There is also an interesting decrease in convection over the far eastern Pacific Ocean that corresponds to enhanced ISO activity over India. The cause for such an increase in mean OLR in the eastern Pacific is not clear.

4.5 Summary and Discussion

Two objective indices that capture the interannual variability of summertime ISO activity over India are developed. One measure is based on EOF analysis and the other on wavenumber-frequency filtering. Interannual fluctuations in ISO activity are largely due to variations in the number of active and break periods from one year to the next rather than shifts in the characteristic ISO period. Seasons of high ISO activity tend to contain significantly more low rainfall days than seasons

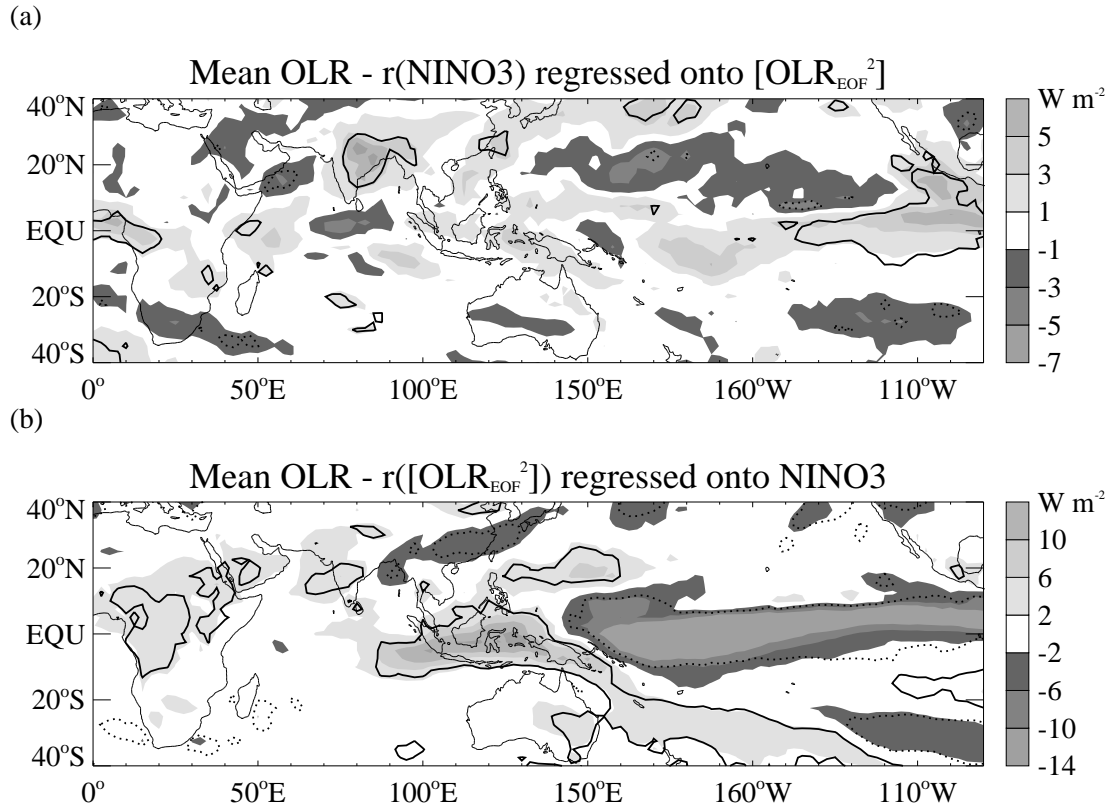


Figure 4.20. Regression of June–September mean OLR onto (a) $[\text{OLR}_{\text{EOF}}^2]$ and (b) Niño3 SST for the 22-years 1975–1997 (excluding 1978). Prior to forming the regressions, OLR that is (a) linearly dependent on Niño3 SST and (b) linearly dependent on $[\text{OLR}_{\text{EOF}}^2]$ is removed. OLR anomalies are shown for a 1.5σ anomaly of $[\text{OLR}_{\text{EOF}}^2]$ and Niño3 SST, respectively. Black lines outline regions where correlation coefficients are significant at the 95% level based on 22 degrees of freedom (± 0.36).

devoid of ISO activity, particularly over land. Furthermore, the seasonal ISO activity is inversely correlated, at approximately -0.55 , with measures of Indian monsoon strength. The high frequency of break days during strong ISO activity seasons may be the major contributing factor that determines the total reduced summer rainfall during those seasons.

Singh *et al.* (1992), who examined ISO activity by analyzing 80 years of daily station rainfall data, conclude that there is no relationship between ISO activity and seasonal mean Indian rainfall, a result that contradicts the findings of this study. One possible reason for the contradiction may be due to decadal changes in ISO activity. Slingo *et al.* (1999) found that global ISO activity was markedly reduced in the period 1958–1976 compared to recent years. A significant reduction in the level of global ISO activity could contribute to lower correlations between ISO activity and Indian rainfall during those periods, and hence overall correlations.

Correlations between ISO activity and JJAS Niño3 SST, and global SST anomalies for that matter, are low. There is some indication that the small positive correlations are the result of enhanced (reduced) early southwest monsoon season ISO activity during the warm (cool) phase of ENSO. The lack of any clear relationship between ISO activity and global SST anomalies (see also Slingo *et al.* 1999; Hendon *et al.* 1999) implies that interannual variability of ISO activity is either internally generated or is forced by land surface conditions. Hendon (1999) argues that a weak Australian monsoon could enhance wintertime ISO activity by shifting the mean convection distribution closer to the equator which presumably is a more favorable condition for ISO formation (e.g., Wang and Li 1994; Salby *et al.* 1994). Such a sequence of events may also occur during summer with a weak continental Indian monsoon permitting stronger ISO activity. However, the

deepest off-equatorial monsoon convection lies over the Bay of Bengal where interannual changes in OLR are relatively unresponsive to interannual shifts in ISO activity (correlation of -0.18). Therefore, some seasons that are characterized by strong off-equatorial ISO activity are also characterized by large regions of deep off-equatorial convection that theoretically would inhibit ISO activity. In any case, correlations between monsoonal convection and ISO activity are not overwhelmingly large which points to the likelihood that interannual fluctuations of ISO activity may be internally and chaotically generated. A potentially important caveat to this conclusion is the observation that the ISO activity exhibits strong biennial variability (see Fig. 4.9) both visibly and in a simple Fourier spectrum (Fig. 4.21). Confidence in the robustness of the near 2-year spectral peaks is limited due to their proximity to Nyquist frequency. Nonetheless, the near 2-year period stands out well above the remainder of the spectrum, particularly for $[\text{OLR}_{EOF}^2]$. The tropospheric biennial oscillation and the South Asian monsoon seem to be intricately linked (Meehl 1997). The presence of a biennial timescale in ISO activity suggests that it is possible that the TBO is a source of ISO activity variability although a mechanism, apart from the biennial monsoon oscillation, is not readily apparent. The modeling results of Goswami (1995) suggest that the biennial variability of the Indian monsoon could be generated through the interaction of intraseasonal oscillations with the annual cycle.

Whether interannual monsoon variability forces interannual fluctuations of ISO activity or vice versa, the relatively strong inverse correlation between the two phenomena has implications for forecasting. The total explained variance of the summer mean rainfall over India by interannual variations of ISO activity is modest (31%). Nevertheless, the variance explained is of comparable or greater magnitude

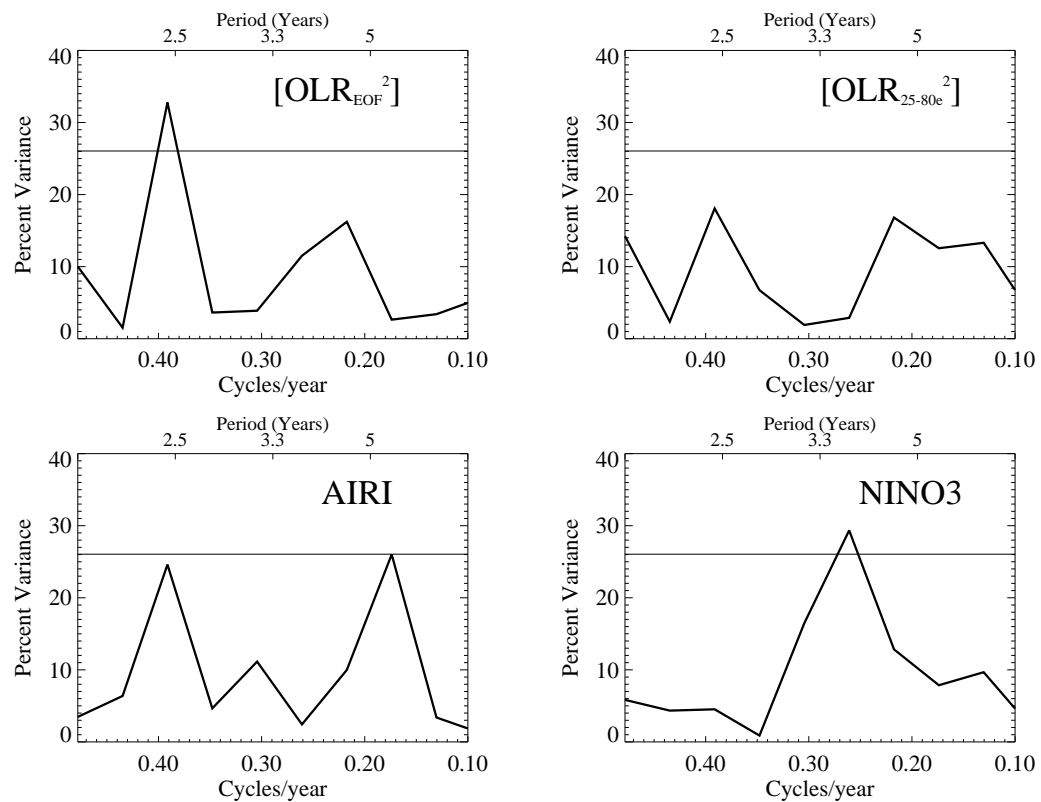


Figure 4.21. Fourier power spectra of $[OLR_{EOF}^2]$, $[OLR_{25-80e}^2]$, AIRI, and JIAS Niño3 SST. Each timeseries is detrended and tapered to zero at the ends with a 20% cosine taper prior to spectral calculations. Thin line shows 95% significance level based on a white noise process.

to that explained by ENSO, at least in the Indian monsoon region. The results presented here point to the need in forecast models for an accurate representation of the ISO, particularly for forecasting weak monsoons when ISO activity is generally strong.

An inconclusive result of this study that is worthy of further attention is the seasonal evolution of summertime ISO activity. According to Figs. 4.5 and 4.6, ISO activity is strongest at the beginning of summer before it tails off over the course of the monsoon season. Additionally, there is limited evidence that the phase of ENSO affects ISO activity in June and July, but not during the rest of the season. Furthermore, dry monsoon seasons that are not also warm ENSO seasons tend to exhibit substantially greater than normal ISO activity during the latter half of the monsoon season. The causes and implications of such intraseasonal variations of ISO activity is not clear and warrants further investigation.